



Cite this: *New J. Chem.*, 2016,  
40, 6276

# Niobium pentoxide nanotube powder for efficient dye-sensitized solar cells

Xiaolin Liu,<sup>a</sup> Renlong Yuan,<sup>a</sup> Yongsheng Liu,<sup>a</sup> Shu Zhu,<sup>b</sup> Jia Lin<sup>\*a</sup> and Xianfeng Chen<sup>\*b</sup>

In this work, we demonstrate for the first time the fabrication of niobium pentoxide (Nb<sub>2</sub>O<sub>5</sub>) nanotube powder using a simple electrochemical anodization method. During the anodization process, the anodic oxide can be continuously and spontaneously released into the electrolyte, and after collection a white powder was obtained. The powder mainly displayed nanotube morphology with the tube length in the range of about 50–100 nm and a diameter of about 20–30 nm. The as-prepared powder was amorphous, and after annealing the powder can be crystallized to the orthorhombic phase. Based on the preparation of the powder, a thick and high quality Nb<sub>2</sub>O<sub>5</sub> film on the transparent conductive substrate was produced, and was further employed as the photoanode in dye-sensitized solar cells (DSSCs). A comparably high efficiency of 3.15% was obtained, with a large open-circuit voltage of 0.738 V, which is among the highest values ever reported for porous Nb<sub>2</sub>O<sub>5</sub> film based DSSCs. Furthermore, the difference in electron behavior of the device as compared to a TiO<sub>2</sub> counterpart was studied, which exhibited a significantly reduced recombination rate, beneficial to high efficiency DSSCs.

Received (in Montpellier, France)  
16th January 2016,  
Accepted 2nd May 2016

DOI: 10.1039/c6nj00159a

www.rsc.org/njc

## 1. Introduction

The development of metal oxide nanostructures other than titanium dioxide (TiO<sub>2</sub>), such as zinc oxide (ZnO),<sup>1,2</sup> tin dioxide (SnO<sub>2</sub>),<sup>3,4</sup> and niobium pentoxide (Nb<sub>2</sub>O<sub>5</sub>)<sup>5–8</sup> for solar energy conversion applications has been recently attracting significant research interest. A Nb<sub>2</sub>O<sub>5</sub> film as a photoanode can provide (1) a higher conduction band energy level than the traditional TiO<sub>2</sub> nanocrystals<sup>9–11</sup> and thus in principle higher open circuit voltage and solar energy conversion efficiency in dye-sensitized solar cells (DSSCs); (2) superior electron properties with smaller interfacial electron recombination,<sup>10</sup> which is essential for liquid and solid-state DSSCs; and (3) better chemical stability. However, DSSCs based on various Nb<sub>2</sub>O<sub>5</sub> nanostructures reported thus far have shown poor performances.<sup>12</sup> A power conversion efficiency of 2.97% was obtained for DSSCs based on Nb<sub>2</sub>O<sub>5</sub> mesoporous spheres through a solvothermal process.<sup>13</sup> The Nb<sub>2</sub>O<sub>5</sub> nanoforest photoanode fabricated by pulsed laser deposition showed 2.41% conversion efficiency.<sup>14</sup> By using electrochemical anodization, a promising method for the synthesis of porous metal oxides, various well-defined Nb<sub>2</sub>O<sub>5</sub> nanostructures on Nb foils have been produced and employed as the photoanode materials in DSSCs. For example, by using thin nanoporous

Nb<sub>2</sub>O<sub>5</sub> networks as the electrode,<sup>15</sup> 4.1% efficiency was achieved with a short-circuit current density ( $J_{sc}$ ) of 10.00 mA cm<sup>-2</sup>, an open-circuit voltage ( $V_{oc}$ ) of 0.70 V, and a fill factor (FF) of 58.5%. For anodic Nb<sub>2</sub>O<sub>5</sub> nanochannels, when utilized in DSSCs, a high efficiency of about 4.5% has been reported,<sup>16</sup> but the fill factor and the open-circuit voltage were poor, with the values of 39.8% and 0.639 V, respectively. To date, the highest efficiency of about 6% has been reported with 11.2 μm thick hydrothermally grown Nb<sub>2</sub>O<sub>5</sub> nanorods.<sup>17</sup>

For anodized Nb<sub>2</sub>O<sub>5</sub> nanostructures, the as-prepared niobium oxides normally tightly adhered to the Nb foil substrate. When employing the oxides for DSSCs, the main problem is that the solar cells based on foil should use the undesired back-side solar cell configuration, which would lead to much energy loss and limited solar cell performance.<sup>18</sup> As has been introduced above, DSSCs based on nanoporous networks and nanochannel structures both used the back-side configuration.<sup>15,16</sup> The anodized Nb oxides free from the metal foil substrate, that is, films coated on transparent conductive oxide (TCO) substrates, can improve light absorption in DSSCs to obtain better performance and will also be more convenient to be utilized in other broad applications. The strategies for TCO substrates with a front-side configuration include direct anodization of sputtered or evaporated Nb films, synthesis and transfer of free-standing membranes, and fabrication of oxide powders. By producing oxide powders,<sup>19</sup> one can simply disperse and coat them onto the TCO substrate to prepare porous oxide films, forming photoanodes for front-side illuminated devices. This strategy is advantageous because it is also

<sup>a</sup> Department of Physics, Shanghai University of Electric Power,  
2103 Pingliang Road, Shanghai 200090, China. E-mail: jlin@shiep.edu.cn

<sup>b</sup> Department of Physics and Astronomy, Shanghai Jiao Tong University,  
800 Dongchuan Road, Shanghai 200240, China. E-mail: xfchen@sjtu.edu.cn

suitable for large-scale production and the film area and thickness can be easily tuned.

Herein, we have performed a simple electrochemical anodization method to directly synthesize Nb<sub>2</sub>O<sub>5</sub> nanotube powder. The morphology, nanostructure, and crystal phase of the obtained powder were characterized in detail. After annealing to induce crystallization, the powder was used as a photoanode material in front-side illuminated DSSCs. Its photoelectric performance and electron properties when applied in DSSCs have been evaluated.

## 2. Experimental

### Preparation of niobium oxide nanotube powder

Niobium oxide powder was prepared by direct electrochemical anodization of niobium metal foil (99.7% purity, J&K Chemical). The electrolyte was 0.74 g NH<sub>4</sub>F and 0.5 g deionized (DI) water added in 50 mL glycerol, and it was mixed by stirring for 2 h before use. The anodization process was performed at a constant voltage of 90 V at room temperature (~25 °C), until the foil was almost completely consumed (before the foil was broken at the electrolyte/air interface). The powder was collected from the anodization electrolyte by centrifugation, washed with ethanol and water 3 times, respectively, and then dried at 120 °C overnight in a drying oven. The powder product was further ultrasonicated in ethanol for 30 min to disperse the powder. To crystallize the powder, it was annealed at 550 °C in air for 4 h (2 °C min<sup>-1</sup>). The morphology of the powder was investigated by field emission scanning electron microscopy (SEM, Hitachi SU8020). The crystal structures were identified by X-ray diffraction (XRD, Rigaku 9KW SmartLab) using Cu K $\alpha$  (wavelength 1.54 Å) radiation from 20–80°. A transmission electron microscope (TEM, Tecnai F30) operating at 300 kV was used to investigate the nanostructure of the powder. A surface characterization analyzer (Micromeritics, 3Flex) was used to measure the surface area of the prepared powder.

### DSSC assembly and characterization

To investigate the application of this Nb<sub>2</sub>O<sub>5</sub> powder in DSSCs with a front-side illumination configuration, Nb<sub>2</sub>O<sub>5</sub> nanotube photoanodes were synthesized. The powder (0.2 g), terpineol, isopropanol, and *n*-butyl alcohol with a mass ratio of 1 : 4 : 1 : 4 were mixed, stirred, and ultrasonicated to make a homogeneous and viscous Nb<sub>2</sub>O<sub>5</sub> paste. The as-prepared paste was coated onto the F-doped SnO<sub>2</sub> (FTO) glass substrate (20  $\Omega$  sq<sup>-1</sup>, 2.3 mm thick, NSG) using a doctor-blade technique. The film thickness was 10  $\mu$ m and the active area was 0.5 × 0.5 cm<sup>2</sup>. The electrode was annealed again at 550 °C in air for 2 h to remove any organic residues, and then sensitized with N3 dye (0.3 mM in ethanol, Solaronix) for 2 days at room temperature (~25 °C). The solar cell assembly and sealing process was the same as reported elsewhere.<sup>19</sup> For comparison, the TiO<sub>2</sub> electrode was prepared using a commercial paste (18NR-T, Dyesol). Intensity modulated photovoltage and photocurrent spectra (IMVS and IMPS) were measured at different light intensities at a wavelength of 470 nm using an electrochemical workstation (Solartron), with  $\pm$ 10%

light intensity modulation and the frequency range from 0.005 to 1 kHz. The open-circuit photovoltage decay (OCVD) measurements were also conducted using the electrochemical workstation. The amount of dye adsorbed was compared by desorbing the dye molecules in 0.1 M NaOH aqueous solution and measuring the absorbance using a UV-Vis-NIR spectrophotometer (UV-3600, Shimadzu). A 3A solar simulator (450 W, Model 94023A, Newport-Oriel Instruments) was used to provide full sunlight (AM 1.5G, 100 mW cm<sup>-2</sup>).

## 3. Results and discussion

### Characterization of niobium pentoxide nanotube powder

The fabrication process of the Nb<sub>2</sub>O<sub>5</sub> nanotube powder is shown in the scheme (Fig. 1a). The field assisted oxidation initiated the formation of niobium oxide on the metal surface. During the process the interfacial barrier layer between the niobium oxide and the metal foil substrate was gradually dissolved and the oxides were released into the electrolyte. And then the formation of niobium oxide through oxidation can be continued. The above processes were repeated, resulting in the periodic formation and release of niobium oxide into the electrolyte. By separating the oxides from the electrolyte, a white oxide powder can be obtained (Fig. 1b), followed by annealing at 550 °C to induce crystallization. The morphology of the synthesized powder was characterized by SEM, as shown in Fig. 1c. By controlling the reaction conditions, dispersed one-dimensional nanotubes were observed, free from the metal substrate. The nanotubes are uniformly distributed, with tube lengths in the range of ~50–100 nm and diameters of ~20–30 nm. This tube structure of the powder is quite different from the arrays or bundles of Nb<sub>2</sub>O<sub>5</sub> nanostructures formed by previous electrochemical anodization.<sup>20,21</sup>

The nanotube morphology of the powder was further studied by transmission electron microscopy (TEM). From the TEM images (Fig. 2a and b), the as-prepared samples showed no obvious

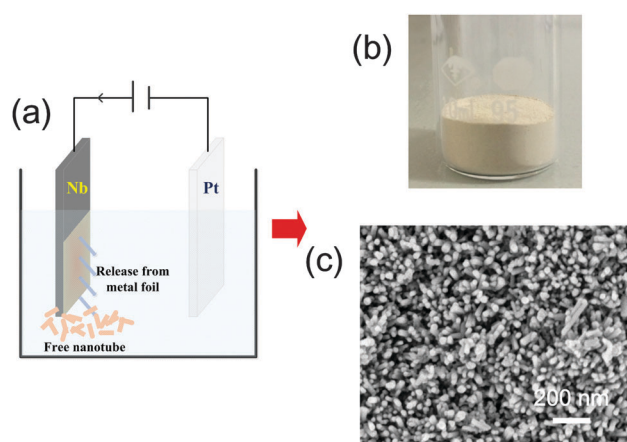


Fig. 1 (a) The scheme of formation of niobium oxide through oxidation and its release to form free nanotubes. (b) The photograph of the collected niobium oxide powder. (c) The SEM image showing the morphology of the powder.

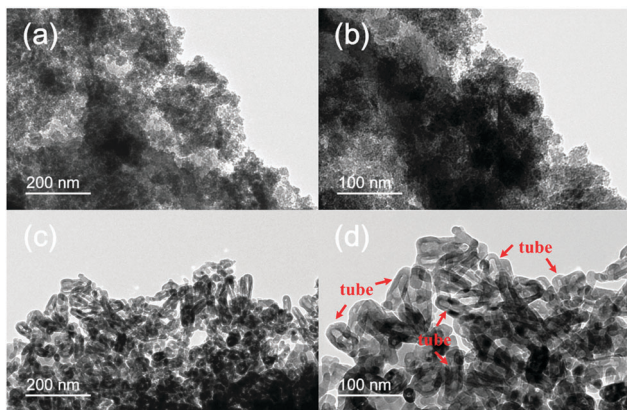


Fig. 2 The TEM images of the (a and b) as-prepared and (c and d) annealed powder samples.

tube morphology. After annealing, the nanotube structure can be clearly observed (Fig. 2c and d), and the tube lengths and diameters are in the range of about 50–100 and 20–30 nm, respectively, in good agreement with the SEM results. Due to the loosely packed nanostructure, the specific internal surface area of the anodic nanotube powder could be much larger than those of the closely packed ones. The Brunauer–Emmett–Teller (BET) measurement showed that the surface area of  $\text{Nb}_2\text{O}_5$  powder before and after annealing was 136.9 and 51.3  $\text{m}^2 \text{g}^{-1}$ , respectively, which is much higher than the surface areas of previously fabricated  $\text{Nb}_2\text{O}_5$  nanostructures by electrochemical anodization (e.g.,  $\sim 14 \text{m}^2 \text{g}^{-1}$  for anodic nanopores).<sup>22</sup> In principle, the network of the nanotubes can provide direct electron pathways and reduce the electron recombination when applied as the photoanode in DSSCs, beneficial to high efficiency solar cells.

The crystal structures before and after annealing were characterized by X-ray diffraction (XRD). The as-prepared nanotube oxide powder after drying appeared to be amorphous without characteristic sharp diffraction peaks (Fig. 3a). As reported previously, the samples synthesized by electrochemical anodization usually have amorphous crystal structures before annealing.<sup>15,16</sup> For DSSC application, the powder was annealed at 550 °C to induce crystallization and to remove any organic residues. After annealing, a highly crystallized powder was obtained with the main diffraction peaks at 22.7°, 28.6°, 36.7°, 46.2°, 50.7°, 55.3°, 58.8°, 64.0°, 71.0° and 78.3° (2-theta). These peaks can be indexed to the orthorhombic phase of  $\text{Nb}_2\text{O}_5$  (JCPDS#27-1003).<sup>23</sup> The crystal structure of the annealed  $\text{Nb}_2\text{O}_5$  nanotube powder was further identified by high resolution transmission electron microscopy (HRTEM) images (Fig. 3b). The highly resolved lattice fringes with spacing  $d = 0.315 \text{ nm}$  was observed, corresponding to the (180) plane of the orthorhombic phase,<sup>24</sup> consistent with the XRD results.

#### Application as a photoanode in dye-sensitized solar cells

As one of the promising photoanode materials, the nanopowder after annealing was investigated for the assembly of DSSCs. Thin films of  $\text{Nb}_2\text{O}_5$  were fabricated by making the powder into a viscous paste and coating it onto a FTO glass substrate using a

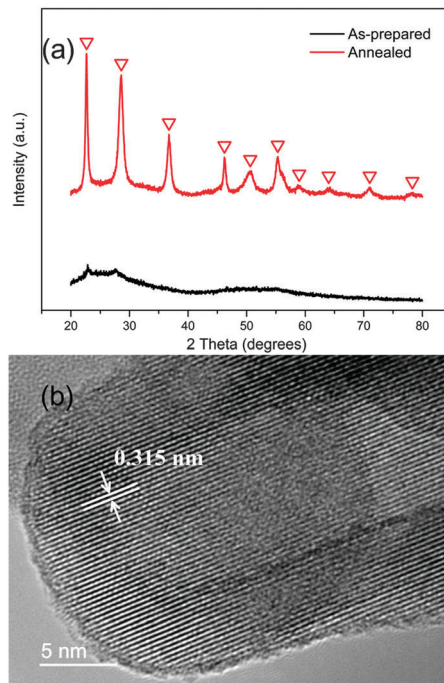


Fig. 3 (a) The XRD patterns of the as-prepared and annealed samples. (b) The HRTEM images of annealed samples.

doctor blade method (see the Experimental section for details), achieving the transparent photoanode for front-side illuminated solar cells. The photographs of the as-prepared photoanode and that after dye infiltration based on the  $\text{Nb}_2\text{O}_5$  powder are shown in the inset of Fig. 4, showing a uniform red color after the dye infiltration. For comparison, the commonly used  $\text{TiO}_2$  nanoparticle film photoanode was also prepared. Both of these films were of the same average thickness of 10  $\mu\text{m}$ . The photoelectric performances of DSSCs based on  $\text{Nb}_2\text{O}_5$  and  $\text{TiO}_2$  photoanodes are shown in Fig. 4. The  $\text{Nb}_2\text{O}_5$  solar cell showed an open-circuit voltage ( $V_{\text{OC}}$ ) of 0.738 V and the  $\text{TiO}_2$  solar cell showed a  $V_{\text{OC}}$  of 0.706 V. The  $\text{Nb}_2\text{O}_5$  solar cell provided an  $\sim 30 \text{ mV}$  increase of  $V_{\text{OC}}$  compared to the  $\text{TiO}_2$  one, and the value is among the highest values ever reported for  $\text{Nb}_2\text{O}_5$  based DSSCs (such as 0.59 V,<sup>25</sup> 0.63 V,<sup>26</sup> 0.70 V,<sup>15</sup> and 0.74 V<sup>17</sup>).

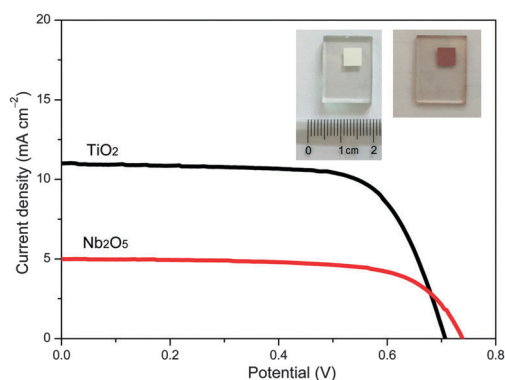


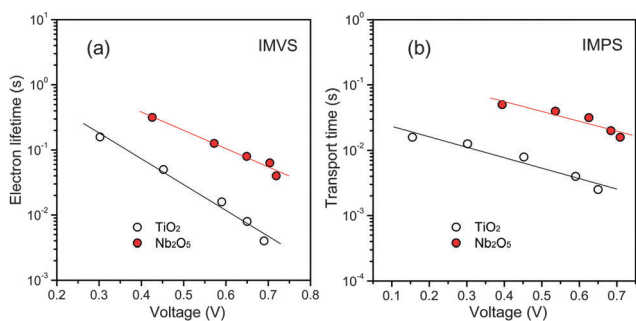
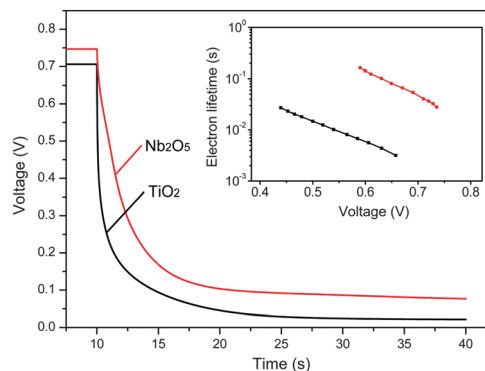
Fig. 4 The current density–voltage ( $J$ – $V$ ) curves of DSSCs based on niobium pentoxide and titanium dioxide electrodes. The inset shows the images of the niobium pentoxide electrode before and after dye adsorption.

**Table 1** The parameters of DSSCs based on Nb<sub>2</sub>O<sub>5</sub> and TiO<sub>2</sub> photoanodes

| Samples                        | V <sub>OC</sub> (V) | J <sub>SC</sub> (mA cm <sup>-2</sup> ) | FF (%) | PCE (%) | Dye amount × 10 <sup>-7</sup> (mol cm <sup>-2</sup> ) |
|--------------------------------|---------------------|--|--------|---------|---|
| Nb <sub>2</sub> O <sub>5</sub> | 0.738               | 6.234                                  | 68.3   | 3.15    | 0.83  |
| TiO <sub>2</sub>               | 0.706               | 11.025                                 | 69.9   | 5.45    | 1.63  |

Although the Nb<sub>2</sub>O<sub>5</sub> cell showed a higher V<sub>OC</sub>, a reduction in photocurrent was observed. The short-circuit current density (J<sub>SC</sub>) was 6.234 mA cm<sup>-2</sup> for the Nb<sub>2</sub>O<sub>5</sub> cell and 11.025 mA cm<sup>-2</sup> for the TiO<sub>2</sub> cell. As the fill factor (FF) was almost the same (68.3% for Nb<sub>2</sub>O<sub>5</sub> and 69.9% for TiO<sub>2</sub>), the photovoltaic conversion efficiency (PCE) of the Nb<sub>2</sub>O<sub>5</sub> cell was 3.15%, lower than that of the TiO<sub>2</sub> cell (5.45%). The detailed parameters are listed in Table 1. We have investigated the dye loading of the Nb<sub>2</sub>O<sub>5</sub> and TiO<sub>2</sub> photoanodes. The loading amount of N3 dye was found to be 0.83 × 10<sup>-7</sup> mol cm<sup>-2</sup> (or the dye molecule number is 0.5 × 10<sup>20</sup> cm<sup>-3</sup>) for Nb<sub>2</sub>O<sub>5</sub> and 1.63 × 10<sup>-7</sup> mol cm<sup>-2</sup> for TiO<sub>2</sub>. The lower dye loading, which was probably due to the mismatch between Nb<sub>2</sub>O<sub>5</sub> and dye,<sup>13</sup> caused the decrease of light harvesting, photocurrent and thus cell efficiency. Thus the further improvement of the efficiency of Nb<sub>2</sub>O<sub>5</sub> cells, *e.g.*, by surface functionalization or structure modification, deserves further exploration.

The electron transport and recombination properties of the Nb<sub>2</sub>O<sub>5</sub> and TiO<sub>2</sub> solar cells were studied using IMVS and IMPS under different illumination conditions.<sup>27,28</sup> Both the effective electron lifetime (τ<sub>n</sub>) and transport time (τ<sub>c</sub>) values reduced exponentially upon increasing the voltage as the electron concentration increased (Fig. 5). In the entire voltage range, the lifetime value was much higher in nanotubular Nb<sub>2</sub>O<sub>5</sub> than in TiO<sub>2</sub>. For example, at the open-circuit voltage of ~0.65 V, the Nb<sub>2</sub>O<sub>5</sub> electrode exhibited >10 times larger lifetime (79.8 ms) than the TiO<sub>2</sub> one (7.5 ms). This implies a reduction in the electron recombination rate with the oxidized species for the Nb<sub>2</sub>O<sub>5</sub> cell with respect to the TiO<sub>2</sub> cell, probably due to less charge transfer and recombination centers existing in the Nb<sub>2</sub>O<sub>5</sub> nanotube powder. The slow electron recombination behavior is beneficial to various applications, *e.g.*, solid-state sensitized and heterostructured solar cells. It is also found that the electron transport time of Nb<sub>2</sub>O<sub>5</sub> was longer than that of TiO<sub>2</sub> (0.021 s *vs.* 0.003 s), which was probably due to the lower

**Fig. 5** The electron lifetime and transport time of the niobium pentoxide and titanium dioxide solar cells as a function of open-circuit voltage.**Fig. 6** The open-circuit photovoltage decay plots. The corresponding effective electron lifetime distribution is shown in the inset.

electronic conductivity of Nb<sub>2</sub>O<sub>5</sub>.<sup>15</sup> As a result of the long lifetime, the charge collection efficiency, calculated as  $\eta_{cc} = 1 - \tau_c/\tau_n$ , is 73.7% for the Nb<sub>2</sub>O<sub>5</sub> cell, higher than that of the TiO<sub>2</sub> cell (60.0%).

The longer electron lifetime and the lower electron recombination rate in the Nb<sub>2</sub>O<sub>5</sub> cell were further confirmed by open-circuit photovoltage decay (OCVD) measurements. The voltage decay behaviors of Nb<sub>2</sub>O<sub>5</sub> and TiO<sub>2</sub> based DSSCs are shown in Fig. 6. The decay rate of the Nb<sub>2</sub>O<sub>5</sub> electrode is obviously lower than the TiO<sub>2</sub> one, indicating slower interfacial electron recombination of Nb<sub>2</sub>O<sub>5</sub> than TiO<sub>2</sub>. The electron lifetime as a function of V<sub>OC</sub> can be calculated using eqn (1).<sup>29</sup>

$$\tau_n = -\frac{k_B T}{e} \left( \frac{dV_{OC}}{dt} \right)^{-1} \quad (1)$$

where  $k_B$  is the Boltzmann constant,  $T$  is the temperature (=298 K), and  $e$  is the electron charge. The result is shown in the inset of Fig. 6. From the OCVD results, the lifetimes of both Nb<sub>2</sub>O<sub>5</sub> and TiO<sub>2</sub> solar cells showed an exponential dependence on V<sub>OC</sub>. The lifetimes of the Nb<sub>2</sub>O<sub>5</sub> cell were more than one order of magnitude higher as compared with the TiO<sub>2</sub> cell at the same V<sub>OC</sub> (*e.g.*, 101.8 ms *vs.* 4.4 ms at ~0.63 V), which is consistent with the IMVS measurement.

## 4. Conclusions

In this work, we have successfully synthesized niobium pentoxide nanotube powder using a simple electrochemical anodization method. The anodically grown niobium oxides can be continuously and spontaneously released from the Nb substrate during the anodization, which were then collected to obtain the oxide powder. The powder showed well-defined nanotube morphology, with uniform tube lengths and diameters and also a large specific surface area. The as-formed powder was amorphous and after annealing an orthorhombic crystal phase was obtained. By utilizing the nanotube powder, we developed the oxide films on a transparent conductive substrate as the photoanode for front-side illuminated dye-sensitized solar cells. The results indicated that the niobium pentoxide solar cell had a high open-circuit voltage and greatly extended electron lifetimes

as compared to the titanium dioxide counterpart, indicating much slower electron recombination. The strategy of the nano-tube powder synthesis is preferable for large-scale production, which may have various potential applications.

## Acknowledgements

The work was supported by the National Natural Science Foundation of China (Grant No. 61125503, 61404081, and 11374204), the Shanghai Municipal Natural Science Foundation (Grant No. 14ZR1417700), and the “Chen Guang” project supported by Shanghai Municipal Education Commission and Shanghai Education Development Foundation (14CG56).

## Notes and references

- M. Law, L. E. Greene, J. C. Johnson, R. Saykally and P. Yang, *Nat. Mater.*, 2005, **4**, 455–459.
- Q. Zhang, T. P. Chou, B. Russo, S. A. Jenekhe and G. Cao, *Adv. Funct. Mater.*, 2008, **18**, 1654–1660.
- K.-N. Li, Y.-F. Wang, Y.-F. Xu, H.-Y. Chen, C.-Y. Su and D.-B. Kuang, *ACS Appl. Mater. Interfaces*, 2013, **5**, 5105–5111.
- S. H. Ahn, D. J. Kim, W. S. Chi and J. H. Kim, *Adv. Mater.*, 2013, **25**, 4893–4897.
- S.-G. Chen, S. Chappel, Y. Diamant and A. Zaban, *Chem. Mater.*, 2001, **13**, 4629–4634.
- M. Wei, Z.-M. Qi, M. Ichihara and H. Zhou, *Acta Mater.*, 2008, **56**, 2488–2494.
- M.-R. Ok, R. Ghosh, M. K. Brennaman, R. Lopez, T. J. Meyer and E. T. Samulski, *ACS Appl. Mater. Interfaces*, 2013, **5**, 3469–3474.
- X. Lin, M. Wu, Y. Wang, A. Hagfeldt and T. Ma, *Chem. Commun.*, 2011, **47**, 11489–11491.
- F. Lenzmann, J. Krueger, S. Burnside, K. Brooks, M. Grätzel, D. Gal, S. Rühle and D. Cahen, *J. Phys. Chem. B*, 2001, **105**, 6347–6352.
- A. Le Viet, R. Jose, M. Reddy, B. Chowdari and S. Ramakrishna, *J. Phys. Chem. C*, 2010, **114**, 21795–21800.
- U. Würfel, M. Peters and A. Hinsch, *J. Phys. Chem. C*, 2008, **112**, 1711–1720.
- R. A. Rani, A. S. Zoofakar, A. P. O’Mullane, M. W. Austin and K. Kalantar-Zadeh, *J. Mater. Chem. A*, 2014, **2**, 15683–15703.
- X. Jin, C. Liu, J. Xu, Q. Wang and D. Chen, *RSC Adv.*, 2014, **4**, 35546–35553.
- R. Ghosh, M. K. Brennaman, T. Uher, M.-R. Ok, E. T. Samulski, L. McNeil, T. J. Meyer and R. Lopez, *ACS Appl. Mater. Interfaces*, 2011, **3**, 3929–3935.
- J. Z. Ou, R. A. Rani, M.-H. Ham, M. R. Field, Y. Zhang, H. Zheng, P. Reece, S. Zhuiykov, S. Sriram and M. Bhaskaran, *ACS Nano*, 2012, **6**, 4045–4053.
- R. A. Rani, A. S. Zoofakar, J. Subbiah, J. Z. Ou and K. Kalantar-zadeh, *Electrochem. Commun.*, 2014, **40**, 20–23.
- H. Zhang, Y. Wang, D. Yang, Y. Li, H. Liu, P. Liu, B. J. Wood and H. Zhao, *Adv. Mater.*, 2012, **24**, 1598–1603.
- J. Y. Kim, J. H. Noh, K. Zhu, A. F. Halverson, N. R. Neale, S. Park, K. S. Hong and A. J. Frank, *ACS Nano*, 2011, **5**, 2647–2656.
- J. Lin, L. Zheng, X. Liu, S. Zhu, Y. Liu and X. Chen, *J. Mater. Chem. C*, 2015, **3**, 6645–6651.
- W. Wei, K. Lee, S. Shaw and P. Schmuki, *Chem. Commun.*, 2012, **48**, 4244–4246.
- H. Jha, R. Hahn and P. Schmuki, *Electrochim. Acta*, 2010, **55**, 8883–8887.
- M. M. Rahman, R. A. Rani, A. Z. Sadek, A. S. Zoofakar, M. R. Field, T. Ramireddy, K. Kalantar-Zadeh and Y. Chen, *J. Mater. Chem. A*, 2013, **1**, 11019–11025.
- H. Luo, W. Song, P. G. Hoertz, K. Hanson, R. Ghosh, S. Rangan, M. K. Brennaman, J. J. Concepcion, R. A. Binstead and R. A. Bartynski, *Chem. Mater.*, 2012, **25**, 122–131.
- P. George, V. Pol and A. Gedanken, *Nanoscale Res. Lett.*, 2007, **2**, 17–23.
- B.-Y. Jeong and E. H. Jung, *Met. Mater. Int.*, 2013, **19**, 617–622.
- R. A. Rani, A. S. Zoofakar, J. Z. Ou, R. A. Kadir, H. Nili, K. Latham, S. Sriram, M. Bhaskaran, S. Zhuiykov and R. B. Kaner, *Chem. Commun.*, 2013, **49**, 6349–6351.
- J. Krüger, R. Plass, M. Grätzel, P. J. Cameron and L. M. Peter, *J. Phys. Chem. B*, 2003, **107**, 7536–7539.
- K. Zhu, N. R. Neale, A. Miedaner and A. J. Frank, *Nano Lett.*, 2007, **7**, 69–74.
- A. Zaban, M. Greenshtein and J. Bisquert, *ChemPhysChem*, 2003, **4**, 859–864.